Swept-source optical coherence tomography of lower limb wound healing with histopathological correlation

Ananya Barui,[a] **Provas Banerjee,**[b] **Rusha Patra,**[a] **Raunak Kumar Das,**[a] **Santanu Dhara,**[a] **Pranab K Dutta,**[a] **and Jyotirmoy Chatterjee**[a]
[a]IIT Kharagpur, School of Medical Science and Technology, Kharagpur, West Bengal 721302 India
[b]Banerjee's Biomedical Research Foundation, 700 005 India

Abstract. Direct noninvasive visualization of wound bed with depth information is important to understand the tissue repair. We correlate skin swept-source–optical coherence tomography (OCT) with histopathological and immunohistochemical evaluation on traumatic lower limb wounds under honey dressing to compare and assess the tissue repair features acquired noninvasively and invasively. Analysis of optical biopsy identifies an uppermost brighter band for stratum corneum with region specific thickness ($p < 0.0001$) and gray-level intensity ($p < 0.0001$) variation. Below the stratum corneum, variation in optical intensities is remarkable in different regions of the wound bed. Correlation between OCT and microscopic observations are explored especially in respect to progressive growth and maturation of the epithelial and subepithelial components. Characteristic transition of uniform hypolucid band in OCT image for depigmented zone to wavy highly lucid band in the pigmented zone could be directly correlated with the microscopic findings. The transformation of prematured epithelium of depigmented area, with low expression of E-cadherin, to matured epithelium with higher E-cadherin expression in pigmented zone, implicated plausible change in their optical properties as depicted in OCT. This correlated evaluation of multimodal images demonstrates applicability of swept-source-OCT in wound research and importance of integrated approach in validation of new technology. © *2011 Society of Photo-Optical Instrumentation Engineers (SPIE)*. [DOI: 10.1117/1.3535593]

Keywords: lower limb wounds; honey dressings; swept-source optical coherence tomography; lucidity; histopathology; E-cadherin.

Paper 10339RR received Jun. 21, 2010; revised manuscript received Dec. 6, 2010; accepted for publication Dec. 17, 2010; published online Feb. 1, 2011.

1 Introduction

Invasive histopathological evaluation is the gold standard for monitoring progress of multistep but overlapping wound healing phases.[1] However, follow-up of this repair process by frequent collection of biopsies after therapeutic intervention is not always feasible.[2] Hence, noninvasive assessment of repairing tissue, especially in full-thickness cutaneous wounds, deserves special attention in regenerative medicine.[3] In this direction, real-time optical coherence tomography (OCT) imaging (the optical biopsy) is gaining popularity with its efficacy in deeper, faster elucidation of epidermal and dermal structures[4–6] at higher resolution in cross sections. It also gets further importance in drawing correlation with histopathological possibilities[7,8] for integrated evaluation. In recent years, the swept-source-OCT (SS-OCT) has emerged to perform tomographic subsurface skin tissue imaging at micron scale and field of view to cover several millimeters. Accordingly, SS-OCT finds an appropriate choice in tomographic imaging of cutaneous wounds because it can generate a high-speed depth profile (up to 2 mm) of the healing bed with micron-level resolution at a sweeping rate of laser with an optimum coherence length of 5–6 mm.[9,10]

In the description of an OCT image, based on relative signal intensity, the term "lucidity" is used analogously to "echogenicity" of ultrasound images. Actually, less hydrated components of tissues reflect more light and are depicted as brighter areas (high lucidity) in contrast to darker areas (low lucidity) with high content of water or fat.[11] Furthermore, the multilayer structure of skin depicts different optical properties according to difference in refractive index, relative thickness, and variation in organic/inorganic components (viz. keratin, water, fat, etc.) of the anatomical sites and regeneration phases.[12–15] Thus, the relatively dehydrated outermost layer of epidermis [i.e., *stratum corneum* (SC)] reflects more light and forms a sharp demarcation line in comparison to the deeper hydrated epidermal layers. In general, the variations in refractive index cause more random scattering and decreases the extent of light penetration into tissues.[2]

Therefore, evaluation of tissue integrity in different regions of the wound bed could be better performed if gray-level intensities of OCT images are assessed through appropriate application of image-processing techniques.[16] Furthermore, due to high resolution and efficacy to reflect the compositional aspects of the tissue in terms of optical properties, these tomographs could be correlated with the histopathological gold standard[2,17] to assess specific biological status of the tissue in health and disease. There are several reports regarding quantitative/semi-quantitative processing of OCT images to achieve meaningful correlation between clinical/histopathological observations. In this regard, Thilo et al.[18] proposed a method for measuring epithelial thickness from OCT and microscopic images. Cobb et al.[19] successfully used an OCT image-based scoring system

in comparison to conventional clinical scoring to define mucosal inflammatory situations.

Furthermore, examining the plausible association of OCT observation with immunohistochemical findings especially in the context of expression of molecules related to the maturation of repairing tissues could be of immense value in evaluating healing stages. In this respect, correlated observation on epithelial expression of E-cadherin, a prime molecule for cell-cell adhesion,[20,21] could be considered in understanding the integrity of regenerated epithelium and the state of maturation.

In this direction, the present study performs *in vivo* SS-OCT imaging on lower limb wound (LLW) regions and analysis thereof. Here, the tomographs are analyzed through the image-processing technique in respect to region-specific variation in the thickness and optical intensity of the SC as well as optical intensity variation in the bands along the vertical direction. Furthermore, it draws a correlation among OCT findings and clinical, histopathological as well as immunohistochemical observations on the wound margin biopsies.

2 Materials and Methods

2.1 Study Design

In this study, 20 patients of both gender (age group of 15–60 years) having traumatic leg wounds from laceration, blunt injury, etc. (nonresponding to conventional treatments) were included under their informed written consent. Clinical examination noted exsudation with pus, foul smell, and necrotic tissues in the wound beds. Wounds were treated with occlusive dressing of honey (i.e., the wound and surrounding inflamed area were covered with honey-soaked sterile cotton gauge, size as per wound bed area, followed by a layer of dry cotton tied with a crepe bandage) on LLW. The redressing was initially performed at 24 h interval for 7–8 days having exsudation and foul odor from the wounds and the duration was further increased to 48–72 h with the healing progression (i.e., formation of granulation tissues, reepithelialization, etc.). The wound beds were photographed before and after 15, 20, and 60 days of intervention by digital camera (Nikon COOLPIX, P80, Japan) to record the debridement of necrotic tissue, granulation tissue formation, and epithelialization in the wound bed. This study was performed under ethical clearance of the institutional ethical committee as per the Helsinki declaration.

2.2 OCT Instrumentation

SS-OCT (OCM1300SS, Thorlabs Incorporated, Newton, New Jersey) incorporates a high-speed frequency-swept external cavity laser (1325-nm central wavelength) with 3-dB spectral bandwidth (BW) ($>$100 nm) and an average output power of 10 mW. It comprises of a Michelson interferometer and a built-in Mach-Zehnder interferometer (MZI, Thorlabs INT-MZI-1300), which provides a frequency clock of the laser. The output laser of Mach-Zehnder interferometer is coupled with a Michelson interferometer to split into the sample and reference path by a broadband coupler (Thorlabs, FC1310–70-50-APC).

In practice, light is focused onto the sample surface by a long-distance objective while maintaining a clearance ($>$25 mm) between optics and sample. An aiming beam (660 nm) is coupled

with the sample arm to locate the scanning trace of the laser. This OCT system could produce high-resolution cross-sectional images for different cutaneous layers with axial and transverse resolutions of 9 and 15 μm, respectively. In this system, the axial scans (A-scans) are performed at a sweeping frequency[9,22] of 16 kHz of laser (100 nm) to construct the depth profile ($\sim$2 mm) at high speed.[23] The interference signal is finally detected using a high-transimpedence gain balanced photodetector having a provision for noise correction. The fast Fourier transform (FFT) is used to convert the time to frequency of the interference signal in yielding a depth-depended profile of OCT images.

2.3 SS-OCT Imaging and Analysis

The OCT scanning (with a 10-mm imaging width) at different regions of the wound bed was performed with a pixel resolution of 8.42 μm (i.e., axial resolution = 12/1.4 = 8.42 μm; where 12 μm is the axial resolution in air and 1.4 is the refractive index of skin) before and after therapeutic intervention. Initially, the OCT gray-scale images [Fig. 1(a)] were converted to binary form using a threshold determined from the histogram.[16] Subsequently, median filtering of size 3$\times$3 and morphological operations (i.e., the opening of A by B is the erosion of A by B, followed by a dilation of the result by B; the erosion and dilation were implemented with a rectangular operator of a 3$\times$3 matrix) were applied.[16] Therein, the connected components were labeled, and the brightest continuous layer was extracted as an SC [Fig. 1(a), panel ii]. The orientation of the extracted SC was further determined using principal component analysis (PCA),[24] which revealed the internal structure of the data in a way that best explains the variance. Finally, the segmented SC was rotated accordingly in the clockwise direction parallel to its x-axis [Fig. 1(a), panel iii]. The vertical thickness for each pixel was calculated and then the average was taken to give the overall thickness of the SC. The intensity was also calculated in a similar way by taking the average of intensity values of each pixel in the SC. In assessing the variation in lucidity along the depth of the SC subtracted images, two distinct regions [i.e., region 1 (25 pixel = 25$\times$8.42 = 210.5 μm, i.e., viable epidermis and upper dermis) and region 2 (50 pixel = 50$\times$8.42 = 421 μm, i.e., rest of the visible dermis)],[16] vertically downward were analyzed in respect to their optical intensity distribution [Fig. 1(b)]. Accordingly, SC segmentation was followed by detection of the upper edge of the SC-subtracted image and, subsequently the above-mentioned regions were demarcated. To study intensity distribution of both the regions, the histograms (Fig. 2) of gray-scale intensity values were plotted for a different area of wound bed. The skewness of the intensity distribution had been assessed by calculating the 50% BW (i.e., 50% fall of the peak value) and 10% BW (i.e., 90% fall of the peak value). Furthermore, for each bandwidth measurement, the deviation of the central value from the peak was calculated. The relative position of the center of 10% BW and 50% BW with respect to peak occurrence characterized the response of the histogram in a robust fashion.

2.4 Histological and Immunohistochemical Studies of Biopsies

Incision biopsies were collected from peripheral tissues of the wound bed under local anesthesia, before and after (i.e., on days 15 and 20) occlusive dressing (honey) intervention.
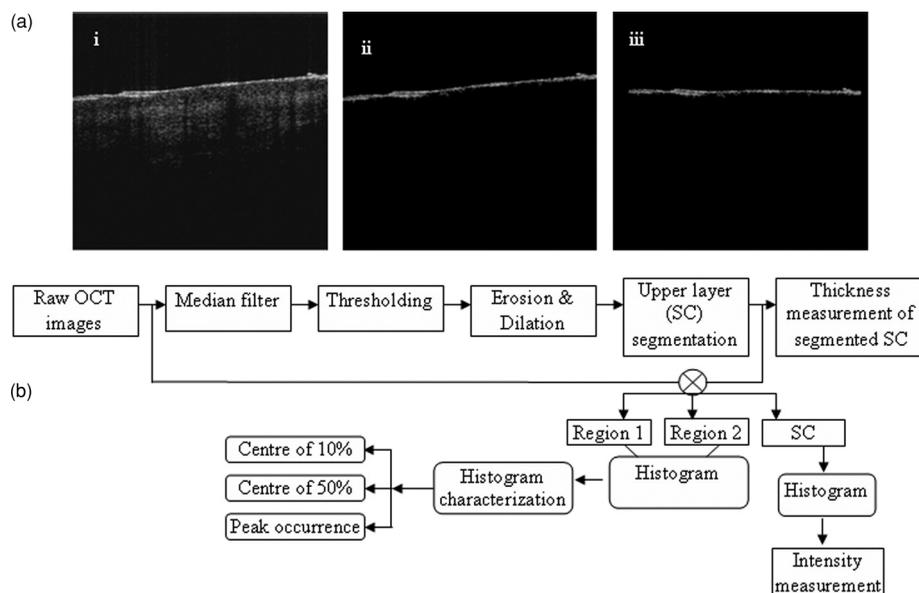
Fig. 1 (a) Panel i shows the original SS-OCT image of healed wound bed area with upper-most bright layer corresponds to SC followed by region 1 (475 μm) for upper epidermis and region 2 (950 μm) for lower epidermis and upper dermis, panel ii shows the segmented out SC, and panel iii shows the rotated SC. (b) Flow diagram of OCT image-processing stages.

The specimens were fixed in 10% phosphate buffered formalin and 4-μm-thick paraffin sections were obtained on poly-L-lysine (Catalog No. P 8920, Sigma-Aldrich, St. Louis, Missouri) coated glass slides for histological (H&E) and immunohistochemical (E-cadherin) studies. In brief, tissue sections were deparaffinized (baking at 60°C) and hydrated for antigen retrieval in a 10-mM citrate buffer (pH 6.0) using the EZ-Retriever System V.2 (BioGenex, San Ramon, California). Sections were blocked using the kit (i.e., Super Sensitive™ Polymer-HRP IHC Detection System Catalog No. QD400–60K BioGenex, San Ramon, California) and incubated overnight at room temperature with primary antibody (E-Cadherin, clone EP700Y, Catalog No. ab40772, Abcam, Cambridge, United Kingdom). Primary binding of antibody was visualized by a HRP conjugated secondary antibody using the chromogen 3, 3'-diaminobenzidine and counterstained with hematoxylin.

Microscopic imaging. The images were grabbed digitally (1388×1040 pixels) by a Zeiss Observer, Z1 microscope (Carl Zeiss, Germany) under 20× (NA 0.8) objectives with 0.31- μm resolution.
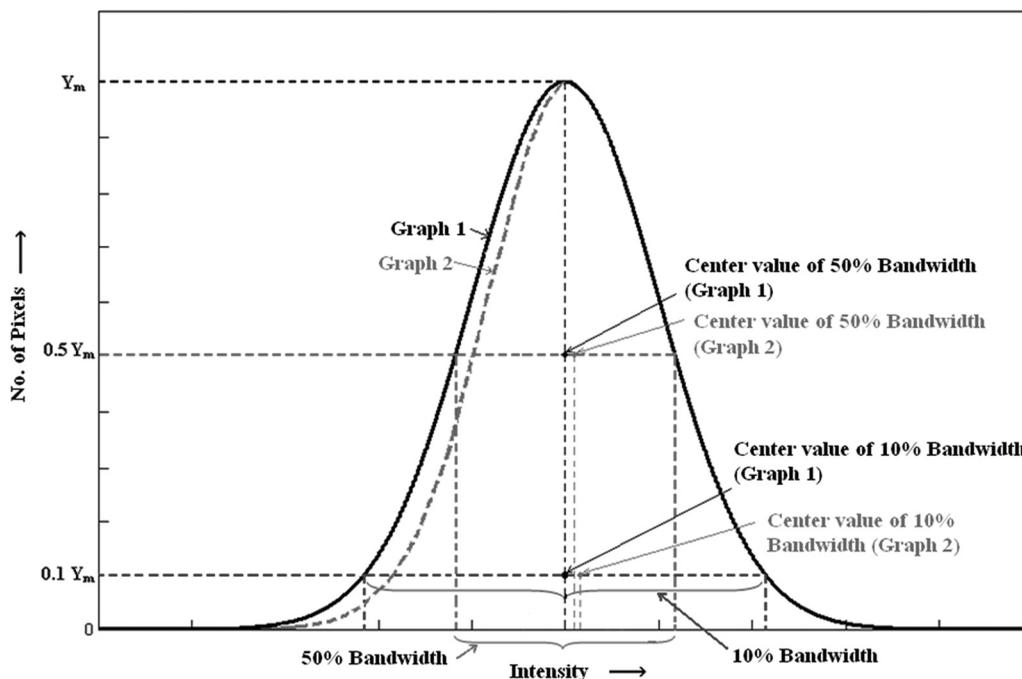

Fig. 2 Graphical representation of bandwidth for the assessment for skewness of gray-scale intensity distribution in SS-OCT images.

Statistical evaluation. The OCT image analysis data were further evaluated to assess their statistical significance using Student's t test.[25]

3 Results

Clinically, it was recorded that the traumatic LLWs progressively healed [Fig. 3(i)–3(iv)] through gradual debridement and optimal granulation tissue formation [Fig. 3(iii)] as well as reepithelialization [Fig. 3(iv)] under honey dressing. Here, it may be noted that the honey facilitates autolytic debridement of the necrotic tissue of the wound bed.[26] Under naked-eye observation, the wound beds could be differentiated into regions such as the unhealed area (with or without necrotic tissues), healed area having depigmented and pigmented zones, and intact skin.

The SS-OCT demonstrated the wound bed region-specific properties of the repaired epithelium (viz. varied optical intensities—lucidity, thickness, appearance of rete-pegs, dermal papillae, etc.) and subepithelial tissue. The unhealed area demonstrated absence of any epithelial feature but depicted tissues with differential lucidity [Fig. 3(a$_1$)]. Whereas, in the depigmented zone, below a highly lucid SC, a uniform low-intensity band of newly formed epithelium was depicted, and this corresponded as the viable epidermis. Below this, a comparatively high lucid zone was observed, representing subepithelial tissues [Fig. 3(b$_1$)]. Through transition of depigmented to pigmented regions, this low-intensity band was gradually reduced [Fig. 3(c$_1$)] and epithelium became comparatively thicker and lucid along with the appearance of rete-pegs and dermal papillae [Fig. 3(d$_1$)]. However, in the intact skin, the contrast between the epithelial and subepithelial zone was reduced in terms of lucidity [Fig. 3(e$_1$)]. The roughness, lucidity, and thickness of the SC layer were maximum in intact skin and minimum in the healed depigmented zone.

The analysis of OCT images, in respect to the SC layer thickness and optical intensities, demonstrated a significant ($p < 0.0001$) interzonal variation (Table 1). The intensity analysis for regions 1 and 2 of the SC-subtracted OCT images demonstrated different intensity distribution in depigmented
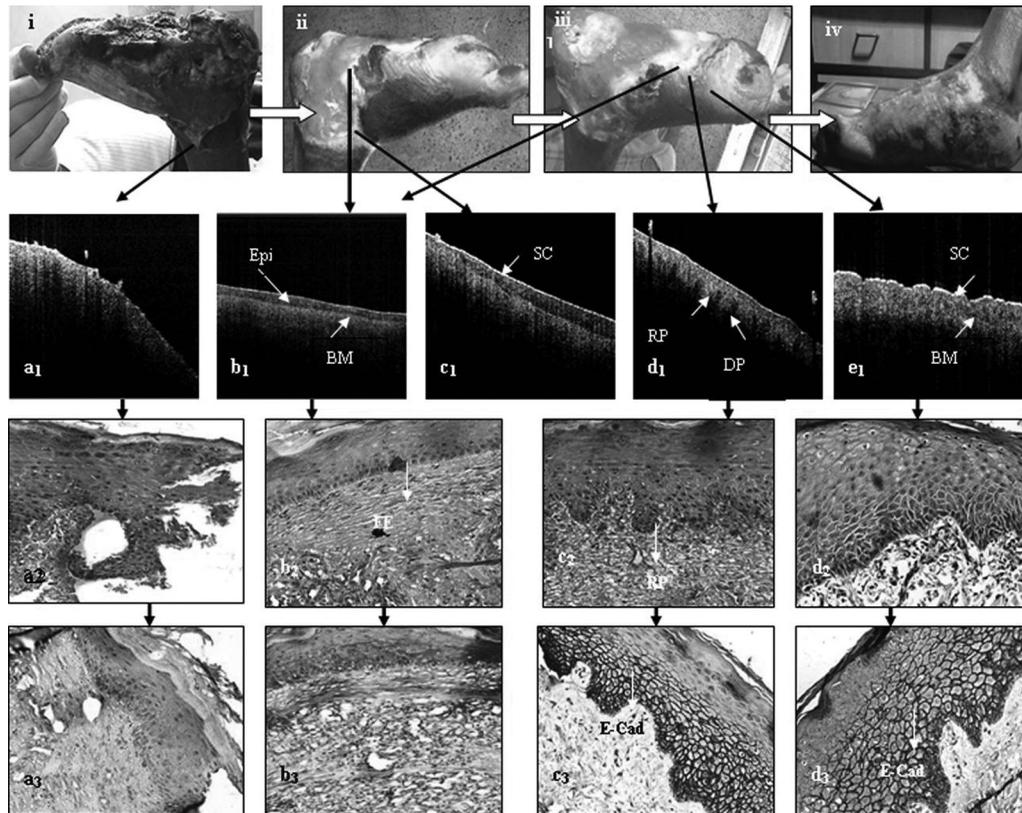

Fig. 3 Depicting multimodal images of LLW at different stages of healing under honey dressing. Clinical photographs (i–iv) represent wound bed on different days: (i) wound with necrotic tissues before therapeutic intervention; (ii–iv) wounds after intervention (ii) showing debridment after 15 days; (iii) after 20 days with granulation tissues, depigmented and pigmented areas; (iv) after 60 days with healed wound bed having patchy pigmented and depigmented areas. (a$_1$–e$_1$) depicted OCT images of different regions of wound bed on 15 days (a$_1$) and 20 days (b$_1$–e$_1$) after healing intervention. (a$_1$) Showing absence of glossy bright SC in the unhealed area, (b$_1$) depigmented area with the features of SC and uniform low optical density (LOD) band followed by high-density zone (HDZ), (c$_1$) transition zone between depigmented and pigmented area of the healed bed with gradual loss of LOD band and increased in HDZ, (d$_1$) pigmented healed area with complete loss of LOD band and appearance of undulation in the SC and alternate LOD and HDZ areas in the lower end of the image, (e$_1$) intact skin with characteristic undulation on SC and broad HDZ. (a$_2$–d$_2$) H&E histopathological photomicrographs of different region of wound bed after healing intervention (20x): (a$_2$) wound margin after 15 days (b$_2$–e$_2$) after 20 days, the depigmented healed area (b$_2$), pigmented healed area (c$_2$) and intact skin (d$_2$). (a$_3$–d$_3$) immunohistochemical photomicrographs of different region of wound bed after healing intervention (20x): (a$_3$) wound margin after 10 days (b$_3$–d$_3$) after 20 days, (b$_3$) the depigmented healed area, (c$_3$) pigmented healed area, and (d$_3$) intact skin. Epi, epithelium; SC; BM, basement membrane; RP, rete-pegs; DP, dermal papillae; FE, flattened epithelium.

Table 1 Average thickness and intensity of SC in SS-OCT image of different regions of healing bed.

Type of skin	ATSC^a ($n = 20$) mean $\pm$ s.d. (μm)	AISC^b ($n = 20$) mean $\pm$ s.d. in relative unit	Feature$^¥$ and p-value
Depigmented skin (DS)	13.64 $\pm$ 0.84	109.43 $\pm$ 4.74	ATSC$^¥$
Transition between pigmented and depigmented (TPD)	24 $\pm$ 3.45	127.05 $\pm$ 8.01	PS versus DS^c
Pigmented skin (PS)	26.61 $\pm$ 3.45	128.47 $\pm$ 4.16	IS versus TPD^c
Intact skin (IS)	29.89 $\pm$ 4.63	138.10 $\pm$ 10.50	IS versus PS^c
			IS versus DS^c
			AISC$^¥$
			PS versus DS^c
			IS versus TPD^c
			IS versus PS^c
			IS versus DS^c

^{a}ATSC = Average thickness of stratum corneum.
^{b}AISC = Average intensity of stratum corneum.
^{c}p < 0.0001.

[Fig. 4(a$_1$)–(a$_2$)] and transitional areas [Fig. 4(b$_1$)–(b$_2$)]. In these areas, region 1 exhibited kurtosis [Fig. 4(a$_1$) and 4(b$_1$)], whereas comparative uniformity was observed for region 2 [Fig. 4(a$_2$) and 4(b$_2$)]. While in the pigmented [Fig. 4(c$_1$)–4(c$_2$)] and intact [Fig. 4(d$_1$)–4(d$_c$)] zones, there was no significant intensity distribution variation. Furthemore, the intensity BW assessment (Table 2) depicted varied properties of the different wound bed regions. In the depigmented area, region 1 displayed nearly the same peak intensity and center values at 50 and 10% BW while in region 2, the histogram was positively (highly) skewed. However, in regions 1 and 2 of the pigmented and intact areas, the center values at 50 and 10% BW were shifted toward left (negatively skewed) wherein, in the transition area although, both histograms were positively skewed but the skewness of region 2 was more.

Histopathological observations [Fig. 3(a$_2$)–3(d$_2$)] noted that in preintervention biopsies, the epithelium of wound periphery was without normal histological features [Fig. 3(a$_2$)]. Although in day 15 and day 20 postintervention biopsies, the depigmented zone depicted flattened, thin epithelium [Fig. 3(b$_2$)] in contrast to the thicker epithelium of the pigmented zone with rete-pegs and features of progressive maturation [Fig. 3(c$_2$)–3(d$_2$)]. In the subepithelial connective tissue of the depigmented zone, the fibers were dense and orientation was less random [Fig. 3(b$_2$)]. However, the fiber density was reduced and orientation became more random in the pigmented and intact zones [Fig. 3(c$_2$)–3(d$_2$)].

The immunohistochemical studies recorded almost no expression of E-cadherin in the epithelium of wound periphery [Fig. 3(a$_3$)] of the preintervention biopsy. In day 15 and day 20 postintervention biopsies, E-cadherin was diffusely expressed

in the flattened epithelium [Fig. (3b$_3$)] of the depigmented zone. However, in the epithelium of the pigmented zone and intact skin, E-cadherin was intensely expressed with a region-specific distribution pattern [Fig. 3(c$_3$)–3(d$_3$)]. In both cases, E-cadherin was diffusely expressed in the basal region, but in other suprabasal layers, it was mostly confined to the cellular membrane.[27,28] Moreover, intact skin depicted maximum E-cadherin expression along the epithelial thickness.

4 Discussion

Finding an analogy between two different imaging modalities is important while correlating their relative performances. In this context, the present study draws a correlation between the SS-OCT findings and microscopic observations on tissue repair. Essentially, SS-OCT is able to deliver high-resolution spatial information, noninvasively, up to $\sim$2 mm of the cutaneous wound bed in terms of lucidity,[9] which varies with tissue composition *vis-à-vis* the stage of tissue maturation.[11]

In the field of dermatology and wound research, OCT observations had been correlated with histological findings, preliminarily.[2,17,19] However, exploring their precise association with epithelial integrity, including related histochemical findings (e.g., E-cadherin expression) in the regenerated tissue of healing wounds, could have great implications to establishing "optical biopsy" as a potent diagnostic tool.

The present SS-OCT observations [Fig. 3(a$_1$)–3(e$_1$)] particularly demonstrated the variation in thickness and lucidity of regenerated wound bed tissues in the respective clinical conditions of LLW healing [Fig. 3(i)–Fig. 3(iii)]. In fact, OCT findings displayed the differences in optical properties of
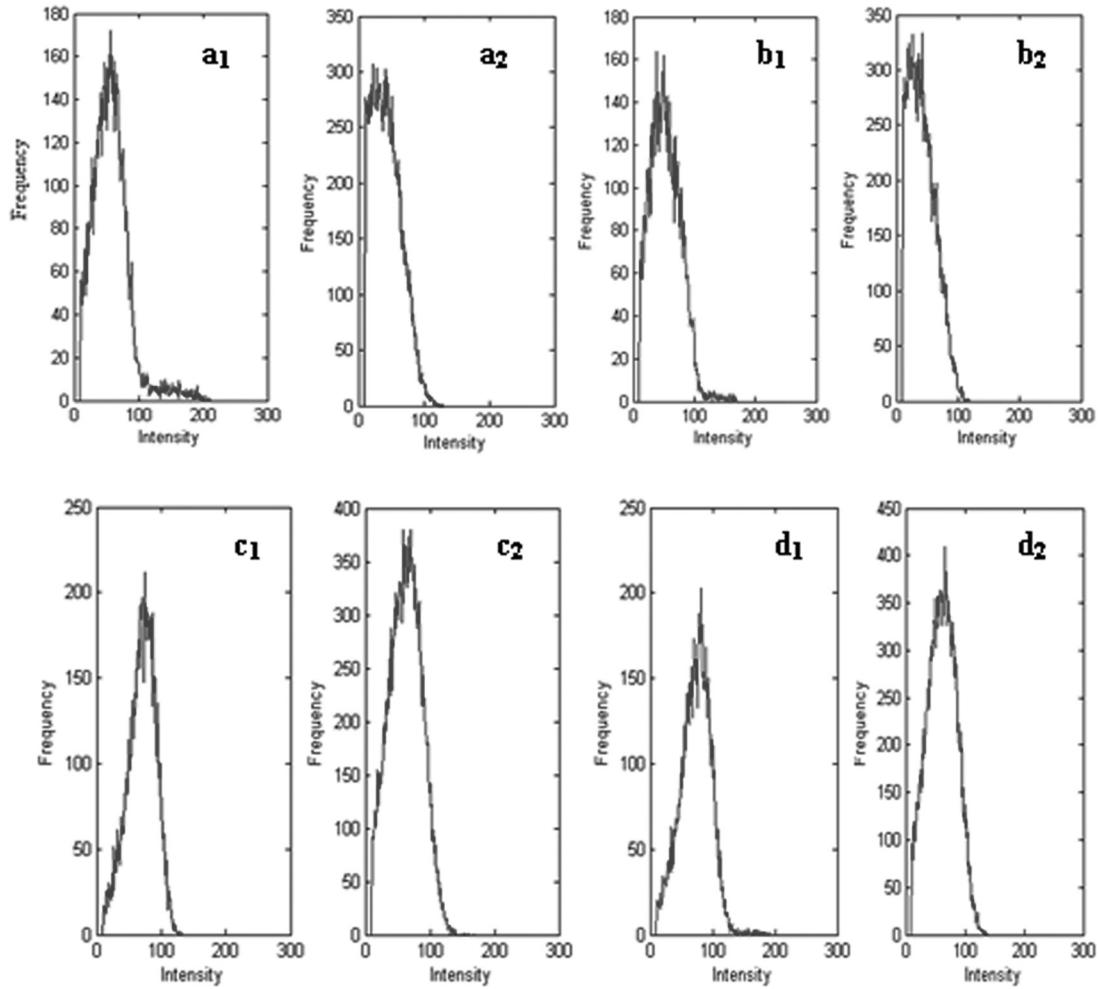
Fig. 4 Intensity distribution of (a_1) region 1, (a_2) region 2 of depigmented skin; (b_1) region 1 and (b_2) region 2 of transitional skin; (c_1) region 1 and (c_2) region 2 of pigmented skin; and (d_1) region 1 and (d_2) region 2 of intact skin.

Table 2 Intensity value of maximum occurrence in different regions of wound bed (see Fig. 2)

Healing bed area	OCT image region	Intensity value of max. occurrence	Intensity values of different BW			
			50% BW	Center value of 50% BW	10% BW	Center value of 10% BW
Depigmented	1	57	54	54	87	53
	2	22	60	39	84	51
Transition between depigmented and pigmented	1	49	64	50	94	56
	2	26	52	35	86	52
Pigmented	1	75	44	53	97	64
	2	70	66	61	108	63
Intact	1	82	48	74	109	66
	2	67	58	59	103	61

unhealed [Fig. 3(a$_1$)], depigmented [Fig. 3(b$_1$)] and pigmented zones [Fig. 3(d$_1$)] as well as intact skin [Fig. 3(e$_1$)] corresponding to their variation in composition and tissue integrity. Likewise, the OCT image [Fig. 3(a$_1$)] depicted absence and presence of the SC in the unhealed and intact skin [Fig. 3(i)], respectively. Although less matured depigmented and transitional areas exhibited the appearance of hypolucid and less thick SC [Fig. 3(b$_1$)–3(c$_1$)] in comparison to matured tissue, i.e., pigmented/intact skin [Fig. 3(d$_1$)–3(e$_1$)]. These were corroborative with the proposition of Ziolkowska *et al.* that the newly formed and matured cutaneous components possess lower and higher lucidity, respectively, due to their corresponding higher and lower hydration states.[11] Perhaps, the presence of hypolucid band in the depigmented area [Fig. 3(b$_1$)], its gradual reduction in the transitional zones [Fig. 3(c$_1$)] and complete disappearance in pigmented [Fig. 3(d$_1$)] as well as in intact skin [Fig. 3(e$_1$)] manifested a direct correlation between the stage of cutaneous tissue maturation and its optical behavior. The hypolucid band actually indicated newly formed flattened epithelium in the regenerated depigmented region with less matured cells, which were replaced by matured cells through healing progression. This fact was further corroborative with SS-OCT findings on the differential optical properties [Fig. 3(d$_1$)] of the epithelial rete-ridges (with higher lucidity) and dermal papillae (with lower lucidity) because water and fat contents are less in the former than in the later.[11]

The explicitness of such image properties was further realized through analysis of their optical intensity distribution and related morphology. The unique revelation by SS-OCT was a significant alteration in SC (Table 1) thickness ($p < 0.0001$), optical intensity ($p < 0.0001$), and surface roughness through the transition of depigmented to pigmented and to intact skin [Fig. 3(a$_1$)–3(e$_1$)]. In this context, the findings of Cobb et al.[19] may be noted where the ultrahigh-resolution OCT was used for evaluating cutaneous wound repair in a mice model for assessing the time-dependent structural and histological changes during healing. The maximum intensity of OCT signals at the tissue surface, noted in their study, was also similar to the current observations. Furthermore, in this work, the intensity histograms of OCT images showed that regions 1 and 2 in depigmented skin were distinct within 75-pixel (i.e., 631.5-μm) depth in contrast to the pigmented and intact skin with more uniformity within the same depth profile. In this direction, the BW analysis of OCT images further revealed the differences between depigmented and pigmented areas in respect to their optical properties (Table 2 and Fig. 4). The kurtosis in region 1 of depigmented and transitional areas [Fig. 4(a$_1$) and 4(b$_1$)] indicated that both the immature regions contained biological components of closely similar optical properties. However, in region 2 of these zones [Fig. 4(a$_2$) and 4(b$_2$)], there was a bias toward lower values (positively skewed), which indicated the presence of mostly hydrated components. Whereas, with comparatively mature areas such as pigmented and intact skin, the overall optical intensities increased (were more lucid) in both regions 1 and 2 [Fig. 4(c$_1$c$_2$) and 4(d$_1$d$_2$)] in comparison to the immature zones, but the intensity distribution was biased toward higher values (negatively skewed), which indicated the presence of more dehydrated components. Thus, such findings distinctly demonstrated the differences in the optical properties of the tissues as per the healing progression and were corroborative with the concept that healed but immature tissues were more hydrated and less reflective (hypolucid) than the mature but dehydrated one.

In drawing correlations between the findings of optical biopsy and incision biopsy, the extent of lucidity and allied morphology in the former could be associated with the microscopic structural and molecular information. Hence, the disappearance of the hypolucid band in OCT vis-à-vis the appearance of epithelial maturation features, such as rete-pegs, dermal papillae, and SC roughness in the pigmented zone of the healing bed, found direct resemblance with histological and immunohistochemical observations. The histological feature of the depigmented zone demonstrated an immature flattened epithelium [Fig. 3(b$_2$)] with low and diffused expression of E-cadherin [Fig. 3(b$_3$)]. Whereas the pigmented and intact skin exhibited a thicker epithelium with microscopic features of progressive maturation and the appearance of rete-pegs [Fig. 3c$_2$) and 3(d$_2$)] as well as a more membranous expression of E-cadherin [Fig. 3(c$_3$) and 3(d$_3$)].

Thus, the recognizable analogy between the OCT and microscopic observations demonstrated the suitability of SS-OCT as a noninvasive imaging tool to explore the maturation stages of different regions of the wound bed as well as the integrity of the regenerated tissues.

5 Conclusions

Therefore, it may be concluded that the SS-OCT images of the different regions of the healing bed could have meaningfully depicted the histopathological possibilities that are confirmed by microscopic evaluation of the wound margin biopsies. Perhaps by exploring the differential optical intensities of repairing tissues, SS-OCT added certain new dimensions regarding integrity of regenerated tissues. This study also demonstrated the exploratory research potential of such an imaging system in understanding the correlation among the morphological feature, optical behavior, and molecular expression of the tissues for a better definition of such biological states. Further studies in this direction may become effective in upholding OCT findings as an alternative to the invasive histopathological observations in wound research.

References

1. F. Strodtbeck, "Physiology of wound healing," *Newborn Infant Nursing Rev.* **1**, 43–52 (2001).
2. R. Steiner, U. Kunzi-rapp, and K. K. Scharffetter, "Optical coherence tomography: clinical applications in dermatology," *Med. Laser Appl.* **18**, 249–259 (2003).
3. G. C. Gurtner, S. Werner, Y. Barrandon, M. T. Longaker, "Wound repair and regeneration," *Nature* **453**, 314–321 (2008).
4. T. Gambichler, G. Moussa, M. Sand, D. Sand, P. Altmeyer, K. Hoffmann, "Applications of optical coherence tomography in dermatology," *J. Dermatol. Sci.* **40**, 85–94 (2005).
5. P. Hrynchak and T. Simpson, "Optical coherence tomography: an introduction to the technique and its use," *Optom. Vis. Sci.* **77**, 347–356 (2000).

6. J. Welzel, "Optical coherence tomography in dermatology: a review," *Skin Res. Technol.* **7**, 1–9 (2001).

7. M. C. Pierce, J. Strasswimmer, B. H. Park, B. Cense, J. F. Boer, "Advances in optical coherence tomography imaging for dermatology," *J. Invest. Dermatol.* **123**, 458–463 (2004).

8. J. Welzel, M. Bruhns, and H. H. Wolff, "Optical coherence tomography in contact dermatitis and psoriasis," *Arch. Dermatol. Res.* **295**, 50–55 (2003).

9. W. C. Kuo, C. H. Chan, C. H. Cho, J. C. H. Cheng, "Swept source optical coherence tomography for radiation-enhanced hepatocellular carcinoma cell invasion imaging," *Phys. Med. Biol.* **54**, 4289–4297 (2009).

10. R. K. Manapuram, V. G. R. Manne, and K. V. Larin, "Development of phase-stabilized swept-source OCT for the ultrasensitive quantification of microbubbles," *Laser Phys.* **18**, 1080–1086 (2008).

11. M. Ziolkowska, C. M. Philipp, J. Liebscher, H. P. Berlien, "OCT of healthy skin, actinic skin and NMSC lesions," *Med. Laser Appl.* **24**, 256–264 (2009).

12. M. A. Calin and S. V. Parasca, "*In vivo* study of age-related changes in the optical properties of the skin," *Lasers Med. Sci.* **25**, 269–274 (2010).

13. M. Huzaira, F. Rius, M. Rajadhyaksha, R. R. Anderson, S. González, "Topographic variations in normal skin, as viewed by in vivo reflectance confocal microscopy," *J. Invest. Dermatol.* **116**, 846–852 (2001).

14. K. P. Nielsen, L. Zhao, J. J. Stamnes, K. Stamnes, J. Moan, "The optics of human skin: aspects important for human health," *Norw. Acad. Sci. Lett.* 35–46 (2008).

15. J. Welzel, C. Reinhardt, E. Lankenau, C. Winter, H. H. Wolff, "Changes in function and morphology of normal human skin: Evaluation using optical coherence tomography," *Br. J. Dermatol.* **150**, 220–225 (2004).

16. R. C. Gonzalez and R. E. Woods, *Digital Image Processing*, Prentice Hall, Englewood Cliffs, NJ (2002).

17. S. C. Whiteman, Y. Yang, and G. D. Pittiu, "Optical coherence tomography: real-time imaging of bronchial airways microstructure and detection of inflammatory/neoplastic morphologic changes," *Clin. Cancer Res.* **12**(3), 813–818 (2006).

18. G. Thilo, B. Stefanie, S. Markus, K. Alexander, S. Michael, M. Georg, A. Peter, H. Klaus. "Comparison of histometric data 455 obtained by optical coherence tomography and routine histology," *J. of Biomed. Opt.* **10**, 44008 (2005).

19. M. J. Cobb, Y. Chen, R. A. Underwood, M. L. Usui, X. Li, "Noninvasive assessment of cutaneous wound healing using ultrahigh-resolution optical coherence tomography," *J. Biomed. Opt.* **11**, (2006).

20. K. F. Becker and B. Luber, "E-cadherin," *UCSD-Nature Molecule* (2010).

21. T. Jakob, M. J. Brown, and M. C. Udey, "Characterization of E-cadherin-containing junctions involving skin-derived dendritic cells," *J. Invest. Dermatol.* **112**, 102–108 (1999).

22. R. Huber, M. Wojtkowski, J. G. Fujimoto et al. "Three-dimensional and C-mode OCT imaging with a compact, frequency swept laser source at 1300 nm," *Opt. Express* **13**, 10523–10538 (2005).

23. <http://www.thorlabs.com/> (date accessed 1 February 2010).

24. R. Duda, P. Hart, and D. Stork, *Pattern Classification*, Wiley, Hoboken, NJ (2007).

25. A. M. Gun, M. K. Gupta, and B. Dasgupta, *An Outline of Statistical Theory*, World Press, Kolkata (2005).

26. M. Subrahmanyam, "Honey dressing for burns—an appraisal," *Ann. Burns Fire Disasters*, **IX**, 33–35 (1996).

27. C. C. Yates, D. Whaley, S. Hooda, P. A. Hebda, R. J. Bodnar, A. Wells, "Delayed re-epithelialization and basement membrane regeneration after wounding in mice lacking CXCR3," *Wound Repair Regen.* **17**, 34–41 (2009).

28. L. G. Hudson, K. M. Newkirk, H. L. Chandler, C.Choi, S. L. Fosseye, A. E. Parente, D. F. Kusewittf, "Cutaneous wound re-epithelialization is compromised in mice lacking functional Slug (Snai2)," *J. Dermatol. Sci.* **56**, 19–26 (2009).